The Huygens entrainment phenomenon and thermoacoustic engines

P. S. Spoor[a] and G. W. Swift
Condensed Matter and Thermal Physics Group, Los Alamos National Laboratory, Los Alamos, New Mexico 87545

(Received 14 September 1999; accepted for publication 1 May 2000)

The earliest known reference to the mode-locking, or entrainment, of two maintained oscillators is Christiaan Huygens' description of two pendulum clocks ''falling into synchrony'' when hung on the same wall. We describe an analogous phenomenon in acoustics—the mode-locking of two thermoacoustic engines which have their cases rigidly welded together, but which are otherwise uncoupled. This ''mass-coupling'' might compete with acoustic coupling when the latter is used to enforce antiphase mode-locking in such engines, for vibration cancellation. A simple theory relating the phase difference between the engines in the locked state to the corresponding ratio of their pressure amplitudes is in excellent agreement with theory and numerical simulations. The theory's prediction relating the phase difference to the engines' natural frequency difference is qualitatively confirmed by experiment, despite larger experimental uncertainties. The mass coupling is relatively weak compared to the aforementioned acoustic coupling, and in general occurs in antiphase, so we conclude that mass coupling will not interfere with vibration cancellation by acoustic coupling in most circumstances. © *2000 Acoustical Society of America.* [S0001-4966(00)01708-2]

PACS numbers: 43.35.Ud, 43.40.Vn [HEB]

INTRODUCTION

Entrainment, or mode-locking, whereby two or more self-maintained oscillators lock together in frequency and phase, exists in a fascinating array of physical and biological systems. The earliest known reference to this phenomenon in the annals of science was made by Christiaan Huygens, who wrote to his father in a letter dated 26 February 1665:[1]

> . . . I have noted an impressive effect which no one has yet been able to explain. This is that two clocks, hanging side by side and separated by one or two feet, keep between them a consonance so exact that the two pendula always strike together, never varying.

In this work we describe the equivalent of the Huygens phenomenon for acoustic resonators. Two cylindrical-duct resonators are welded together side by side, the oscillating gas inside the resonators acting the part of the clock pendula and the duct cases acting the part of the wall upon which the clocks were hung. The resonators exhibit mode-locking in the same way that Huygens' clocks synchronized their motion. The oscillations in the ducts are maintained thermoacoustically, although to observe the Huygens phenomenon, any method of producing spontaneous oscillations will do.

A thermoacoustic engine of a size and power density suitable for heavy industrial applications (such as large-scale natural gas liquefaction[2]) experiences tons of axial dynamic force on its structure from the pressure oscillations of the gas inside it, potentially inducing intense, damaging vibrations in this structure. In a separate paper[3] we show how these vibrations can be canceled by rigidly attaching two engines together, side by side, and acoustically coupling two neighboring ends through a narrow tube a half-wavelength long, thus encouraging the oscillations in the two engines to be in antiphase. If the engines are attached rigidly enough to move as a unit, however, they are of necessity coupled through their mutual structure as well as through the acoustic tube. Hence, our particular goal in the present work was to discover how efforts to cancel external case vibrations in two rigidly attached thermoacoustic engines, by coupling them acoustically, might be helped or hindered by the Huygens-style structural coupling. We refer to this coupling as ''mass coupling,'' since the coupling occurs through forces on a shared mass (the case) and is stronger if the oscillating gas is heavy and the case is light. Therefore, to increase the mass coupling we used a pressurized, heavy gas—xenon—in the lightly constructed engines used for studies of acoustic coupling.[3] Without acoustic coupling, we found that the engines would tend to mass-lock in antiphase, as desired for vibration cancellation. For the range of mass-locked states we could achieve, we measured the dependence of the amplitude ratio of the two engines and the phase difference between them as a function of their natural frequency difference. Even with 3 bars of xenon gas in our engines, the mass-coupling was relatively weak; locked states existed only over a very narrow ''capture bandwidth'' of frequency differences (fractional differences of order 0.001). This article provides a quantitative explanation of these measurements, through both theory and numerical simulations.

I. ESSENTIAL DYNAMICS OF MODE-LOCKING

Two self-maintained oscillators, such as pendulum clocks, organ pipes, or thermoacoustic engines, may alter each other's frequencies enough to lock in frequency and phase if they are sufficiently coupled. When the ''detuning'' (the difference in natural uncoupled frequencies) is large, or

[a]Present address: Clever Fellows Innovation Consortium, 302 10th St., Troy, NY 12180.

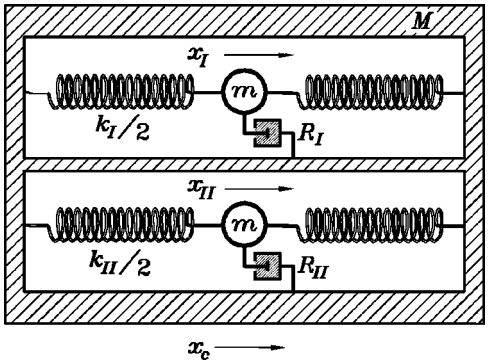

FIG. 1. Mass–spring model of mass-coupled oscillators.

the coupling is weak, the oscillators ''beat'' at the difference frequency, just like coupled linear passive oscillators. As the detuning is decreased, or as the coupling is increased, the beating slows down and eventually stops, at which point the oscillators are locked. The change in frequency of one oscillator depends on its phase relative to the other, so the locked state at a particular detuning is characterized by a corresponding phase difference between the oscillators. In general, the amplitudes in the oscillators also depend on this phase difference, and there may be a net flow of energy from one oscillator to the other if the amplitudes are not equal. In an intermediate state, where the coupling is not quite strong enough to lock the oscillators, they beat with a nonsinusoidal envelope—the beat period elongates when the frequencies have a close approach.

We use the following notation for two oscillators that are mode-locked or nearly mode-locked:

$$\psi_{\mathrm{I}}(t)=\Re\{\Psi_{\mathrm{I}}(t)e^{i[\omega t+\phi_{\mathrm{I}}(t)]}\}, \tag{1}$$

$$\psi_{\mathrm{II}}(t)=\Re\{\Psi_{\mathrm{II}}(t)e^{i[\omega t+\phi_{\mathrm{II}}(t)]}\}, \tag{2}$$

where $\Re\{\}$ indicates taking the real part. Here $\psi_{\mathrm{I,II}}$ could be displacements, pressures, velocities, or any other similar variables of interest that depend on time t. We assume that the amplitudes $\Psi_{\mathrm{I,II}}$ and the phases $\phi_{\mathrm{I,II}}$ are real and slowly varying compared to the angular frequency ω, and $\Psi_{\mathrm{I,II}}\geqslant 0$. The locked state is characterized by a relative phase between the oscillators and a ratio of their amplitudes, which are

$$\phi=\phi_{\mathrm{II}}-\phi_{\mathrm{I}}, \quad \zeta=\frac{\Psi_{\mathrm{II}}}{\Psi_{\mathrm{I}}}. \tag{3}$$

We assume that oscillator I has natural frequency ω_{I} and oscillator II has ω_{II} when I and II are uncoupled, so that the difference in natural frequencies, or detuning, is

$$\Delta\omega=\omega_{\mathrm{II}}-\omega_{\mathrm{I}}. \tag{4}$$

We let the compromise frequency ω that the oscillators possess when they are coupled be a constant in time; the apparent *instantaneous* difference in frequency between resonators II and I is simply $\Delta\omega_{\mathrm{inst.}}=\partial\phi/\partial t$.

The obvious mechanism for frequency shift in our system is the moving case. If a simple harmonic oscillator of mass m and stiffness k is anchored to an unfettered mass M, the natural frequency is shifted according to

$$\omega_0^2=\frac{k}{m}\left(1+\frac{m}{M}\right). \tag{5}$$

For a straight cylindrical half-wave acoustic resonator whose case of mass M is free to move, the corresponding expression is [see Sec. II B, especially Eqs. (32) and (36)]

$$\omega_0^2\simeq\frac{\pi^2a^2}{l^2}\left[1+\left(\frac{8}{\pi^2}\right)\frac{m_g}{M}\right], \quad m_g\ll M, \tag{6}$$

where $\pi a/l$ is the natural angular frequency of a half-wave resonator with sound speed a and length l, and m_g is the total mass of gas in the resonator. Thus one might conclude that the effective mass of the oscillating gas in a half-wave resonator is $m=(8/\pi^2)m_g\simeq 0.8m_g$ in the present context.

II. THEORY

A. Mass-and-spring model

Before discussing coupled acoustic engines, we will consider a simple system of masses and springs, arranged to resemble two mass-coupled acoustic resonators. Figure 1 shows a pair of mass–spring oscillators that attach to the same moving mass. The oscillators are identical except for a slight difference in frequency; they have masses m and springs k_{I} and k_{II}, hence also natural frequencies $\omega_{\mathrm{I}}=\sqrt{k_{\mathrm{I}}/m}$ and $\omega_{\mathrm{II}}=\sqrt{k_{\mathrm{II}}/m}$. Following Pippard[4] and Van der Pol,[5] the feedback mechanism that maintains the oscillations is modeled by a resistance that can be either positive or negative, depending on the amplitude. We let

$$R_{\mathrm{I}}=\frac{m\omega_{\mathrm{I}}}{Q}\left(1-\frac{X_0^n}{X_{\mathrm{I}}^n}\right), \tag{7}$$

where X_{I} is the amplitude in oscillator I and X_0 is the steady-state amplitude to which the oscillator relaxes. Recall from Sec. I that the amplitude X_{I} is assumed to vary slowly with time compared to ω. The equation of motion for oscillator I in the absence of coupling is then

$$\ddot{x}_{\mathrm{I}}+\omega_{\mathrm{I}}^2x_{\mathrm{I}}+\frac{\omega_{\mathrm{I}}}{Q}\left(1-\frac{X_0^n}{X_{\mathrm{I}}^n}\right)\dot{x}_{\mathrm{I}}=0, \tag{8}$$

where $x_{\mathrm{I}}(t)$ is the displacement of the mass m from equilibrium, and the dot indicates a time derivative. We use this particular form because if X_0 is set to zero, one obtains the equation for an ordinary damped oscillator, with Q akin to the quality factor of the oscillator.

The exponent n depends on the mechanism maintaining the oscillations. Here, we argue that a thermoacoustic engine is governed by $n=2$ when comparing steady-state amplitudes at different operating points. In the mass-and-spring model, the power delivered or absorbed by the oscillator (the ''load'') is $\dot{W}_L=-(m\omega/Q)(1-X_0^n/X^n)|\dot{x}|^2$. In a thermoacoustic engine, such things as resonator dissipation and stack power are also proportional to amplitude squared,[6] so the power produced by the stack is $\dot{W}_{\mathrm{stack}}=\beta P_0^2=\beta P^2+\dot{W}_L$, where P_0 is the unloaded pressure amplitude and P is the loaded amplitude. Then we have $\dot{W}_L=\beta P_0^2-\beta P^2$, or $\dot{W}_L=-\beta(1-P_0^2/P^2)P^2$.

In practice, we find that only the ratio Q/n, and not Q or n separately, can be measured experimentally (and therefore, for our purposes, Q/n is all that matters). In principle, one should be able to determine both Q and n from transient measurements; however, the thermal mass of a thermoacoustic engine causes the growth and decay time constants to be artificially long. The ratio Q/n that governs the steady state can be measured by comparing states at various loads, but if we consider only small loads (i.e., $P \approx P_0$, or $X \approx X_0$) such as the engines experience when they are coupled, it is difficult to distinguish Q or n separately.

To fully analyze the dynamics of the system, we could write down the equations of motion with full time dependence, carry out the time derivatives in these equations, with $x(t)$ having the form suggested by Eqs. (1) and (2), and find expressions for $\partial\phi/\partial t$ and $\partial\zeta/\partial t$. Pippard[7] treats a problem very similar to ours in this manner. However, we are interested mostly in locked states, where everything is in the steady state. We seek expressions for the state variables ϕ and ζ in terms of known or measurable quantities like m, M, Q, and $\Delta\omega$, and an expression for the ''sensitivity'' of the system, $\partial\phi/\partial\Delta\omega$. This last quantity is of particular interest in the vibration-cancellation context, because it tells how fast a system tends to move away from some ideal phase (e.g., $\phi=\pi$) as it is detuned; when considering a mode-locked pair of acoustic engines, a movement of phase away from $\phi=\pi$ means more case vibration.

One may readily show, as has Pippard,[7] that a reactively coupled pair of oscillators like ours has two possible locked states, one nominally near $\phi=0$ and one nominally near $\phi=\pi$. Which one is actually selected is of some interest; a tendency for our coupled engines to mass-lock at $\phi=0$, where both ''masses'' are moving in the same direction, could impair vibration cancellation. Fortunately, we may take some comfort in the words of Huygens[1] describing his mode-locked pendulum clocks:

> . . . the motion of the pendula, while they are in consonance, are not in phase, but they approach and fall back with contrary motion . . .

Due to external friction on our moving case, we expect the mode with the least case motion to be favored. In a passive, linear system, the modes that experience more damping tend to decay faster, and we expect similar behavior in our system, although it is neither passive nor strictly linear. In any event, like Huygens, we nearly always observe that our engines mass-lock in antiphase rather than in-phase. [If one extracts the mechanisms from two metronomes and mounts them on a very light balsa-wood or perforated-aluminum frame, and suspends this frame so it is free to swing, the Huygens phenomenon is readily observable. One of us (PS) has experimented with such a system, observing both in-phase and antiphase locking of the metronomes, the former especially if the two metronome pendula are initially started out with in-phase motion.]

To proceed with our analysis, then, we will let $d/dt = i\omega$, and assume amplitudes and phases are constant in time. We obtain

$$(\omega_{\mathrm{I}}^2-\omega^2)X_{\mathrm{I}}+\frac{i\omega\omega_{\mathrm{I}}}{Q}\left(1-\frac{X_0^2}{X_{\mathrm{I}}^2}\right)X_{\mathrm{I}}=\omega_{\mathrm{I}}^2 e^{i(\phi_c-\phi_{\mathrm{I}})}X_c\,, \tag{9}$$

$$(\omega_{\mathrm{II}}^2-\omega^2)X_{\mathrm{II}}+\frac{i\omega\omega_{\mathrm{II}}}{Q}\left(1-\frac{X_0^2}{X_{\mathrm{II}}^2}\right)X_{\mathrm{II}}=\omega_{\mathrm{II}}^2 e^{i(\phi_c-\phi_{\mathrm{II}})}X_c\,, \tag{10}$$

$$-\omega^2 X_c=\mu\omega_{\mathrm{I}}^2(e^{i(\phi_{\mathrm{I}}-\phi_c)}X_{\mathrm{I}}-X_c)+\mu\omega_{\mathrm{II}}^2(e^{i(\phi_{\mathrm{II}}-\phi_c)}X_{\mathrm{II}}-X_c), \tag{11}$$

where $\mu=m/M$. Referring to Fig. 1, note that X_c is the motion amplitude of the common mass, and hence the right sides of Eqs. (9) and (10) are coupling terms. Equation (11) can be solved for X_c; substituting this result in Eqs. (9) and (10) yields

$$(\omega_{\mathrm{I}}^2-\omega^2)+\frac{i\omega\omega_{\mathrm{I}}}{Q}\left(1-\frac{X_0^2}{X_{\mathrm{I}}^2}\right)=-\mu(\omega_{\mathrm{I}}^2+\omega_{\mathrm{II}}^2\,\zeta\, e^{i\phi})\,, \tag{12}$$

$$(\omega_{\mathrm{II}}^2-\omega^2)+\frac{i\omega\omega_{\mathrm{II}}}{Q}\left(1-\frac{X_0^2}{X_{\mathrm{II}}^2}\right)=-\mu(\omega_{\mathrm{II}}^2+\omega_{\mathrm{I}}^2 e^{-i\phi}/\zeta)\,. \tag{13}$$

We assume that $\mu \ll 1$ and $|1-X_0^2/X_{\mathrm{I,\,II}}^2| \ll 1$, and that $\omega_{\mathrm{II}} \sim \omega_{\mathrm{I}} \sim \omega$. Taking the real part of Eq. (13) minus Eq. (12), keeping terms to first order, and simplifying gives

$$\frac{\Delta\omega}{\omega}=\frac{\mu}{2}(\zeta-1/\zeta)\cos\phi\,. \tag{14}$$

To find a second equation, we follow Pippard[7] and assume that in the steady state, energy is conserved in the system, i.e.,

$$\frac{m\omega_{\mathrm{I}}}{Q}\left(\frac{X_0^2}{X_{\mathrm{I}}^2}-1\right)|\dot{x}_{\mathrm{I}}|^2+\frac{m\omega_{\mathrm{II}}}{Q}\left(\frac{X_0^2}{X_{\mathrm{II}}^2}-1\right)|\dot{x}_{\mathrm{II}}|^2=0\,. \tag{15}$$

[Equation (15) may also be obtained from the ratio of the imaginary parts of Eqs. (12) and (13).] After some algebra, this leads to the identity

$$\frac{X_0^2}{X_{\mathrm{I}}^2}-\frac{X_0^2}{X_{\mathrm{II}}^2}=\frac{1}{2}\left(\zeta^2-\frac{1}{\zeta^2}\right)\,. \tag{16}$$

Using this identity, with the imaginary part of Eq. (12) minus Eq. (13), yields

$$(\zeta-1/\zeta)=2\mu Q\sin\phi\,. \tag{17}$$

Equations (14) and (17) can be combined to eliminate ζ, to obtain

$$\frac{\Delta\omega}{\omega}=\mu^2 Q\sin\phi\cos\phi\,; \tag{18}$$

in the limit $\phi\to\pi$, this leads to

$$\frac{\omega}{\pi}\frac{\partial\phi}{\partial\Delta\omega}=\frac{1}{\pi\mu^2 Q}\,. \tag{19}$$

This last equation is particularly useful for comparing the present results with those for acoustically coupled engines.[3]

The results in this section are simple and roughly true for any mass-coupled pair of oscillators. In the next section, to obtain results specific to mass-coupled acoustic engines,

we will derive differential equations isomorphic with Eqs. (9)–(11) for the acoustic pressure in the engines and the forces on the case. We will derive equations valid for engines with resonators of arbitrary cross section, and then modify these for specific examples of interest.

B. Acoustic model

Consider two nearly identical acoustic engines, called engines I and II, which are rigidly attached side-by-side and have a combined case mass M. Each engine consists of a prime mover section, where heat is applied and the acoustic power to sustain the oscillations is generated, and a resonator section, which comprises the bulk of the volume and is mostly responsible for determining the frequency at which the engine runs. The engine cross section may vary with position, but the radius is always much smaller than the length l. The engines are also assumed to be supporting what is more or less a half-wavelength mode. The long axis is labeled x, and is positive in the same direction as positive displacements and positive forces. The prime movers are located near the $x=0$ end, and we assume the acoustic pressure at the $x=l$ end is known.

We assume that the acoustic pressure throughout each engine as a function of x and t can be written as a product of the pressure $p(t)$ at the $x=l$ end and a spatial weighting function $w(x)$, that is,

$$\text{pressure}_{\text{I}}(x,t)=w(x)p_{\text{I}}(t)\,, \tag{20}$$

$$\text{pressure}_{\text{II}}(x,t)=w(x)p_{\text{II}}(t)\,. \tag{21}$$

Furthermore, in the manner of Eqs. (1) and (2), we assume

$$p_{\text{I}}(t)=\Re\{P_{\text{I}}e^{i(\omega t+\phi_{\text{I}})}\}\,, \tag{22}$$

$$p_{\text{II}}(t)=\Re\{P_{\text{II}}e^{i(\omega t+\phi_{\text{II}})}\}. \tag{23}$$

Following Morse,[8] and guided by the results in Sec. II A, we write the inhomogeneous wave equation for engine I as

$$p_{\text{I}}\nabla^2 w-w\ddot{p}_{\text{I}}/a^2-\frac{\omega_{\text{I}}}{Q}\left(1-\frac{P_0^2}{P_{\text{I}}^2}\right)w\dot{p}_{\text{I}}/a^2=-\rho\dot{s}\,, \tag{24}$$

where a is the sound speed, ρ is the density, and the source density $s(x,t)=(1/V)\partial V/\partial t$ is the volume velocity per unit volume imposed by the moving boundaries. Multiplying both sides by $-wa^2$ and integrating over the volume leads to

$$\ddot{p}_{\text{I}}-\frac{\int_V a^2 w\nabla^2 w\,dV}{\int_V w^2\,dV}p_{\text{I}}+\frac{\omega_{\text{I}}}{Q}\left(1-\frac{P_0^2}{P_{\text{I}}^2}\right)\dot{p}_{\text{I}}=\rho a^2\frac{\int_V \dot{s}w\,dV}{\int_V w^2\,dV}. \tag{25}$$

(Note that ρa^2 is a constant, so it appears outside the integral.) This last equation has exactly the same form as Eq. (8), if the right-hand side is zero (no coupling), with the coefficient of p_{I} identified as ω_{I}^2. [In the limit that a is constant, and ∇w is zero at the walls, the vector identity $\nabla\cdot(w\,\nabla w)=(\nabla w)^2+w\,\nabla^2 w$ and Gauss' theorem (for turning the volume integral of a divergence into a surface integral) yield

$$-\frac{\int_V a^2 w\nabla^2 w\,dV}{\int_V w^2\,dV}=\frac{a^2\int_V(\nabla w)^2 dV}{\int_V w^2\,dV}=\omega_{\text{I}}^2, \tag{26}$$

in accordance with Rayleigh's principle relating the frequency of a normal mode oscillation to the ratio of the maximum potential and kinetic energies.[9,10]] Hence, an appropriate equation for p_{I} is

$$\ddot{p}_{\text{I}}+\omega_{\text{I}}^2 p_{\text{I}}+\frac{\omega_{\text{I}}}{Q}\left(1-\frac{P_0^2}{P_{\text{I}}^2}\right)\dot{p}_{\text{I}}=\rho a^2\frac{\int_V \dot{s}w\,dV}{\int_V w^2\,dV}. \tag{27}$$

To make this equation specific to mass coupling, consider how the moving case of an acoustic resonator couples to the gas inside. If the motion of the resonator is essentially rectilinear, then (in the low-amplitude limit) changes in cross section act like local volume-velocity sources (or sinks). In a cylindrical resonator of varying cross-sectional area $A(x)$, one may write

$$s(x,t)=\frac{1}{A(x)}\frac{dA(x)}{dx}u_c(t), \tag{28}$$

where u_c is the case velocity in the x direction, which is the same for all x (if the case is assumed rigid). We can also find u_c in terms of the forces on the case; considering the forces exerted by *both* engines, assuming they are identical in geometry, and neglecting viscous forces, we can write

$$\dot{u}_c=-\frac{p_{\text{I}}+p_{\text{II}}}{M}\int_0^l\frac{dA(x)}{dx}w\,dx, \tag{29}$$

where M is the total case mass. Note that for each *abrupt* change in cross section, say between $x_j-\varepsilon$ and $x_j+\varepsilon$,

$$\int_{x_j-\varepsilon}^{x_j+\varepsilon}\frac{dA(x)}{dx}w\,dx=[A(x_j+\varepsilon)-A(x_j-\varepsilon)]w(x_j)\,. \tag{30}$$

For example, Eq. (30) would apply to the endcaps of a typical resonator. Combining Eqs. (27)–(29), and using $\int_V\{\}dV=\int_0^l\{\}A\,dx$, we obtain

$$\ddot{p}_{\text{I}}+\omega_{\text{I}}^2 p_{\text{I}}+\frac{\omega_{\text{I}}}{Q}\left(1-\frac{P_0^2}{P_{\text{I}}^2}\right)\dot{p}_{\text{I}}=-\frac{\rho a^2}{M}\frac{[\int_0^l(dA/dx)w\,dx]^2}{\int_0^l w^2 A\,dx}p_{\text{I}}(1+\zeta e^{i\phi}). \tag{31}$$

We may now make use of the results previously obtained for the mass–spring system. Starting with Eq. (31) for p_{I} and a similar equation for p_{II}, letting $d/dt=i\omega$, and then dividing the first equation by $p_{\text{I}}(t)$ and the second by $p_{\text{II}}(t)$ results in a pair of equations exactly like Eqs. (12) and (13), except that the constant $\mu\omega^2$ has been replaced by a more complicated expression. We can therefore identify the effective mass ratio μ for the acoustic system as

$$\mu=\frac{\rho a^2}{\omega^2 M}\frac{[\int_0^l(dA/dx)w\,dx]^2}{\int_0^l w^2 A\,dx}, \tag{32}$$

and then all the results obtained for the mass–spring system should apply to the acoustic system as well.

1. Obtaining Q of engines from experiment

We measure Q from the ''load response'' of each engine. Suppose that instead of a moving case, the only volume-velocity source is a small orifice at $x=l$ (e.g., a

valve) leading to a small volume, forming an acoustic RC network which serves as a load. In the steady state, the differential equation for the loaded engine leads to

$$(\omega_0^2-\omega^2)\tilde{p}+i\omega\frac{\omega}{Q}\left(1-\frac{P_0^2}{P^2}\right)\tilde{p}=-\rho a^2\frac{i\omega\tilde{U}_e}{\int_0^l w^2 A\,dx}, \tag{33}$$

where $\tilde{p}$ is the complex pressure amplitude at the loaded end of the resonator, P is its magnitude, and $\tilde{U}_e$ is the volume velocity exiting that end. Multiplying both sides by $\tilde{p}^*/i\omega$, where $\tilde{p}^*$ is the complex conjugate of $\tilde{p}$, and taking the real part leads to

$$\frac{\omega}{Q}(P^2-P_0^2)=-\left[\frac{2\rho a^2}{\int_0^l w^2 A\,dx}\right]\Re\{\tilde{p}^*\tilde{U}_e\}/2. \tag{34}$$

Since $\Re\{\tilde{p}^*\tilde{U}_e\}/2=\dot{W}_L$, the time-averaged load on the engine, it follows that

$$Q=-\left[\int_0^l w^2 A\,dx\right]\frac{\omega}{2\rho a^2}\left(\frac{\partial P^2}{\partial \dot{W}_L}\right). \tag{35}$$

(In this context, power flowing out of the engine is positive; for constant heat input to the engine, pressure amplitude drops as the load increases, so $\partial P^2/\partial\dot{W}_L$ is negative.)

Strictly speaking, the left side of Eq. (35) should be $2Q/n$, but this is moot unless one can find n independently, say by measuring the curvature of P^2 vs $\dot{W}_L$. We find that for the engines in the present work, P^2 vs $\dot{W}_L$ is quite linear, and the data have sufficient scatter to discourage higher-order fitting. Since $n=2$ simplifies some of the math, it is a useful assumption. The interested reader may verify that carrying out our derivations with arbitrary n leads to the same results as ours, but for the appearance of $2Q/n$ instead of Q (as long as $P_{\mathrm{I,II}}\approx P_0$).

2. Uniform-diameter engine

To enable ready comparison of theory to numerical simulations in a later section, we consider the simple example of an engine with a single cross-sectional area A_0 throughout. If we further assume that the pressure distribution in such an engine is simply $w(x)=-\cos(\omega/a)x$, then $\int_0^l (dA/dx)w\,dx=-2A_0$ and $\int_0^l w^2 A\,dx=A_0 l/2$. Our formulas for μ and Q become

$$\mu=\frac{8\rho a^2 A_0}{\omega^2 lM}=\frac{8}{\pi^2}\frac{m_g}{M} \tag{36}$$

and

$$Q=\frac{\omega A_0 l}{4\rho a^2}\left(\frac{\partial P^2}{\partial\dot{W}_L}\right)=\frac{\omega}{2\rho^2 a^2}\frac{m_g}{2}\left(\frac{\partial P^2}{\partial\dot{W}_L}\right), \tag{37}$$

where $m_g=\rho A_0 l$ is the mass of gas in the engine and ρ and a are assumed constant.

3. Application to acoustic coupling

A useful check on part of our theory is to compare its predictions for *acoustic* coupling with those published in Ref. 3. The sensitivity to frequency difference of two engines coupled by a narrow half-wavelength tube of area A_c is[3]

$$\left(\frac{\omega}{\pi}\right)\frac{\partial\phi}{\partial\Delta\omega}\bigg|_{\text{acoust.}}=F_{\mathrm{H}}\frac{\pi}{4}\left(\frac{A_\tau}{A_c}\right)\frac{\delta}{r_c}, \tag{38}$$

where r_c is the radius of the coupler and δ is the effective thermoviscous boundary layer thickness $\delta=\delta_\nu+(\gamma-1)\delta_\kappa$; δ_ν is the viscous penetration depth, δ_κ is the thermal penetration depth, and γ is the ratio of isobaric to isochoric specific heats. F_{H} is a quantity called the ''Helmholtz factor,'' which is proportional to $1/A_\tau$ but depends only weakly on r_c and δ. A_τ is arbitrary and normally refers to a typical cross-sectional area of the engines; if the engines have a constant cross section A_0, then choosing $A_\tau=A_0$ makes $F_{\mathrm{H}}=1$. The Helmholtz factor represents the effect on sensitivity of nonuniform cross section, e.g., of using engine geometries that are more like Helmholtz resonators and less like straight ducts. Combining our present general theory with that of Ref. 3, we may find F_{H} analytically. A full expression for F_{H} that is precisely accurate over a wide range of coupler diameters has a very complicated dependence on r_c, δ_κ, and δ_ν, but reasonable accuracy is obtained with

$$F_{\mathrm{H}}=\frac{2}{A_\tau l_c}\int_0^l w^2 A(x)\,dx, \tag{39}$$

which is exact in the limit $r_c\gg\delta$, $l_c\to\lambda/2$, where l_c is the resonant coupler length and λ is the wavelength. In this limit, Eq. (39) predicts $F_{\mathrm{H}}=2.83$ for the engines in the present work, letting A_τ equal the endcap area at $x=l$ and performing the integral numerically using a DELTAE[11] simulation of a single engine (with air at 80 kPa as the working gas). For comparison, our DELTAE simulation of two acoustically coupled engines predicts $F_{\mathrm{H}}=[(\omega/\pi)\partial\phi/\partial\Delta\omega]/[(\pi/4)A_\tau/A_c(\delta/r_c)]=2.80$, a difference of only 1%. We may also compare our present theory with the experimental results in Ref. 3; in that work, two sets of sensitivity data were obtained, one on the engines used in this work (which have a variable cross section—see Fig. 4) and another on engines that were nearly uniform in cross section. The geometry of the engines was the only thing that varied between the two experiments, so if A_τ is chosen to be the same for both types of engine, the ratio of the measured sensitivities should be

$$\frac{\text{sensitivity (var. } A)}{\text{sensitivity (const. } A)}=\frac{F_{\mathrm{H}}(\text{var. } A)}{F_{\mathrm{H}}(\text{const. } A)}=\frac{\int_0^l w^2 A(x)\,dx\ (\text{var. } A)}{A\int_0^l w^2\,dx\ (\text{const. } A)}. \tag{40}$$

This formula predicts a ratio of 3.09, whereas the data and simulations in Ref. 3 both indicate a ratio of 3.08, a negligible difference.

III. COMPARING THEORY WITH NUMERICAL SIMULATION

To compare our theory with numerical simulations, we used DELTAE[11] to model a mass-coupled pair of engines with uniform cross section. DELTAE (Design Environment

for Low-amplitude ThermoAcoustic Engines) integrates the one-dimensional wave equation in the small-amplitude (''acoustic'') approximation, including thermal and viscous effects, according to the thermoacoustic theory of Rott.[12] To simulate a mass-coupled pair of engines, we force all four endcaps in the model to move with the complex case velocity, and require that the case acceleration be the complex sum of all the end pressures times the cross-sectional area, divided by the case mass (we ignore forces on the heat exchangers and stack). We then vary ω_{II} relative to ω_{I} by varying the ambient gas temperature inside simulated engine II, and note the effect on the phase difference ϕ between the engines and on their amplitude ratio ζ. The results of this simulation may be compared to the predictions of Eqs. (17)–(19), using Eqs. (36) and (37) for μ and Q. In order to obtain Q, we simulate a single engine with no moving endcaps, and a large real impedance instead of a perfectly rigid endcap at $x=l$. As the end impedance is lowered, the power flowing out of the end increases and the pressure drops; the derivative $\partial P^2/\partial \dot{W}_L$ is therefore obtained.

While these simulated engines have a simple shape, we strive to make them similar in other respects to the real engines we studied. The simulated engines are filled with 3 bar of xenon, with an ambient temperature of 300 K; they run at 56 Hz and have $Q\approx 200$ and $m_g\approx 0.06$ kg; they are 1.6 m long and have $A_0\approx 2.3\times 10^{-3}$ m^2. They are also set to run with cold-end acoustic pressure of about 16 kPa, since this is close to where our experimental engines were operated.

First, we will compare the Q that best describes the simulated mode-locked states according to Eq. (17) with the Q determined by observing the simulated load-response of one engine as suggested by Eq. (37). By combining the two equations, as well as Eq. (36) for μ, one may obtain the putative identity

$$\frac{\zeta-1/\zeta}{\sin\phi}=\frac{4A_0^2}{\omega M}\left|\frac{\partial P^2}{\partial \dot{W}_L}\right| . \tag{41}$$

The quantities on the left-hand side define the locked state, and the quantities on the right are well-defined constants that are independent of the locked state, if we restrict our attention to the limit $\phi\to\pi$, $\dot{W}_L\to 0$. In our simulations, everything is held constant but Q; for each point, the exact pore geometry of the stack is altered slightly to change the performance of the engine (i.e., change $\partial P^2/\partial \dot{W}_L$). We find that over the range $70\leqslant Q\leqslant 230$, there is virtually no difference between the left and right sides of Eq. (41). These Q values are similar to those of our actual devices, and typical of the passive Q's of acoustic resonators with geometry and gas properties similar to our engines.

Next, we may inquire whether the sensitivity $\partial\phi/\partial\Delta\omega$ of our simulated system matches theory. We use Eq. (19), along with Eqs. (36) and (37) for μ and Q, and compare that result to the value of $(\omega/\pi)\partial\phi/\partial\Delta\omega$ suggested by the simulations in the limit $\phi\to\pi$. In order to make a meaningful comparison, we must address one subtlety, that of calculating $\Delta\omega$, the difference in natural frequencies of two acoustic engines. This question has direct bearing on our experiments as well. One can imagine defining the ''natural frequency'' of an engine as the natural resonance of a column of gas with the engine's geometry and temperature distribution, or as the frequency with which an engine with that geometry and temperature distribution will run. When the frequency difference between two engines is largely determined by the temperature of the gas in the resonators, the distinction between these definitions is unimportant; but when two engines are weakly coupled, even a very small change in frequency can mean a relatively large change in phase, which can mean a significant change in the acoustic power flow between the engines. This in turn can cause significant differences in the engines' hot-end temperatures, and these differences can ultimately dominate the frequency difference. In this circumstance, the difference in the running frequencies of the two engines may vary considerably from the difference in their gas-column resonance frequencies.

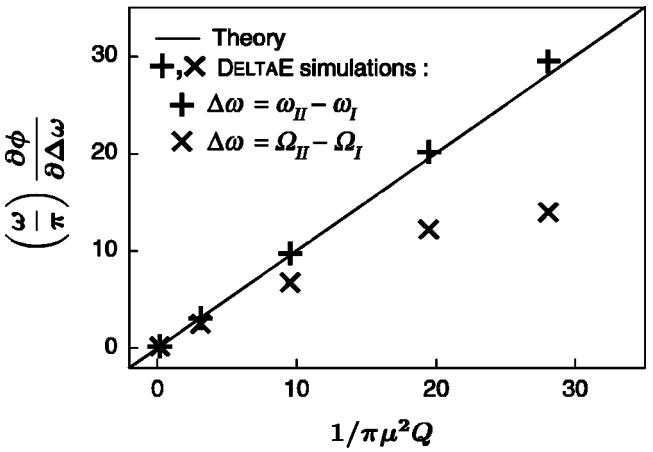

FIG. 2. The sensitivity $\partial\phi/\partial\Delta\omega$ of a pair of mass-locked thermoacoustic engines with uniform cross section, as predicted by theory (line) and DELTAE simulation (symbols).

This distinction is of little practical importance in the big picture, since one is generally more interested in how sensitive the locked states are to objective external changes (one engine sitting in the sun, the other in the shade; one engine driving a bigger load, etc.) and not to changes in the ''natural frequencies,'' particularly if those frequencies are dominated by the engines' internal responses to external changes. However, the natural frequency difference is a very convenient analytic tool, and useful for expressing general results about mode-locked systems—e.g., the phase difference ϕ between the engines is determined by $\Delta\omega$, however that $\Delta\omega$ comes about.

We compare our theory with simulation by calculating the frequency difference two ways; the first, $\Delta\omega=\omega_{\mathrm{II}}-\omega_{\mathrm{I}}$, is the difference in the gas-column resonances; the second, $\Delta\omega=\Omega_{\mathrm{II}}-\Omega_{\mathrm{I}}$, is the difference between the frequencies at which the engines will run, uncoupled, if they have the same temperature distribution as when coupled.

Figure 2 shows the comparison of simulations and theory; moving along the horizontal axis from left to right, the coupling is weakened by increasing the mass M of the combined engine cases, thereby lowering μ, but leaving Q unchanged. As the coupling gets weaker, $\Omega_{\mathrm{II}}-\Omega_{\mathrm{I}}$ overestimates the value of $\Delta\omega$. Therefore we might expect that in an experiment on a weakly coupled system, the values of ζ and

ϕ for a given locked state might agree well with theory, but the experimentally determined $\partial\phi/\partial\Delta\omega$ will be smaller than its ''true'' value.

Acoustically coupling[3] two engines so that they lock near $\phi=\pi$, and keeping $|\phi-\pi|$ small enough so that 95% of the case vibration is canceled when their frequency difference is as much as 1%, leads to $(\omega/\pi)\partial\phi/\partial\Delta\omega\approx 2$. Typically, an engine might have $Q\sim 100$ and $\mu\sim 10^{-3}$, implying that the mass-coupled sensitivity is $(\omega/\pi)\partial\phi/\partial\Delta\omega = 1/\pi\mu^2 Q\approx 10^4$. This implies that the mass coupling is really very weak, and can be ignored in the vibration-cancellation application. Absent heroic efforts, we are confined to weakly coupled engines in the laboratory as well. The engines we use for our experiments are charged with 3 bar of xenon (as in the simulations) and lightly constructed; still, we find that $1/\pi\mu^2 Q\approx 10^3$.

A. Possible complications

In many presentations on mode-locking, few quantitative results are given because it is usually so difficult to estimate the coupling strength. In Huygens' workshop, his clocks could have been coupling by uniform motion of the wall, elastic waves in the wall, or even motion of the nearby air. (Huygens himself suggested that it was the ''imperceptible agitation of the air caused by the motion of the pendula'' that enabled the clocks to ''communicate.''[1]) In addition, one would have to characterize the ''load response'' of the clock mechanism to obtain the coupling strength.

By contrast, we can successfully characterize the coupling of our thermoacoustic engines, given the nature of the analytic results and our experience at making acoustic and thermodynamic measurements. To illustrate how difficult the problem can become, however, and why it often is not worth the effort to make quantitative analyses of mode-locked systems, we will consider two of many possible subtle complications: external dissipation on the case and heat leak between the engines' hot ends.

1. External dissipation

So far we have treated the coupling between the engines as purely reactive, but we know the actual coupling impedance must be richer in detail, and in particular it must contain some resistance. One possible consequence of external resistance (friction in the engine mounts, etc.) is that it may discourage the $\phi\simeq 0$ mode. In an extreme limit, imagine that the case mass becomes negligible and the only impedance is a dashpot connecting the case to a rigid wall. Obviously the mode that encourages maximum motion of the dashpot will suffer more damping than the mode that encourages minimum motion. This may help explain why the in-phase, $\phi\simeq 0$ mode was rarely observed by us (or Huygens). There are other, more subtle consequences of adding resistance to the coupling, however.

Consider the mass-and-spring model of Fig. 1. Imagine connecting one side of a dashpot with mechanical resistance R_c to the case M, and the other side to a rigid wall, so that the coupling impedance $Z_c=R_c+i\omega M=\omega M(i+\alpha)$, where $\alpha=R_c/\omega M$. The additional dissipation alters the analysis presented in Sec. II A. A new term $i\omega^2\alpha X_c$ is added to the left side of Eq. (11), with consequences in Eqs. (12)–(14). The energy conservation equation, Eq. (15), becomes

$$(X_0^2-X_{\rm I}^2)+(X_0^2-X_{\rm II}^2)=\frac{\alpha Q}{\mu}X_c^2, \tag{42}$$

with consequences in Eq. (16). Equation (17) becomes

$$\zeta-1/\zeta=\frac{2\mu Q\sin\phi}{1+\alpha^2+\alpha\mu Q}. \tag{43}$$

Finally, in the limit $\phi\to\pi$, and with the approximation $\zeta+1/\zeta\approx 2$ (which is true for our experimental system, but is *not* generally true for all systems far from the center of the ''capture band''), we find

$$\frac{\omega}{\pi}\frac{\partial\phi}{\partial\Delta\omega}=\frac{1}{\pi\mu^2 Q}\left[\frac{1+\alpha^2+\alpha\mu Q}{1+\alpha/\mu Q}\right]. \tag{44}$$

Recall from Eq. (19) that without external resistance, the sensitivity $(\omega/\pi)\partial\phi/\partial\Delta\omega=1/\pi\mu^2 Q$, so we may view everything in the square brackets on the right side of Eq. (44) as the effect of external resistance on sensitivity. Figure 3 shows this multiplying factor as a function of α, for a number of different values of μQ.

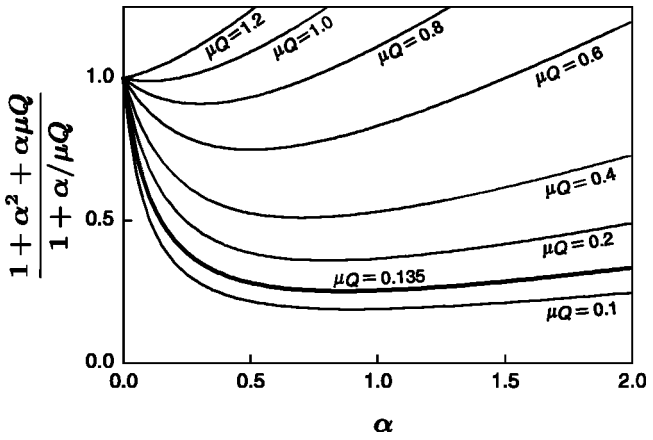

FIG. 3. Normalized sensitivity of a mass-locked system with external resistance R_c as a function of $\alpha=R_c/\omega M$, for various strengths of mass coupling. The darker line corresponds to $\mu Q=0.135$, the value we estimate for our experimental system of coupled thermoacoustic engines.

The behavior of these curves is not immediately intuitive. For strong coupling (large μQ) the addition of dissipation increases the sensitivity, making the system more weakly coupled; but for systems that are weakly coupled already, the addition of small amounts of external damping actually *enhances* the coupling, quite dramatically. (For our acoustic engines, this suggests that adding a small real component to the coupling impedance results in a phasing, between the pressure at the endcaps of the resonator and the case motion, that is more favorable to energy transfer between the engines.) Each curve has a minimum at $\alpha=1-\mu Q$, if $\mu Q\leqslant 1$. Only after the resistance becomes fairly large does the coupling strength begin to diminish again. This could have quite a noticeable effect on any ϕ vs $\Delta\omega$ data.

In contrast, Eq. (43) is only a small perturbation away from Eq. (17), for small external resistance. In addition, the

perturbation appears only as a multiplicative constant, so it is virtually impossible to tell from ζ vs ϕ data whether there is external dissipation, as opposed to whether one's values for μ and/or Q are inaccurate.

We have not pursued this much further, or tried to devise a reliable method for measuring R_c. In principle, one can determine it from measurements of case motion; that is, the phase between the motion of the case and the pressures inside may indicate whether the pressure forces are driving a reactance or a reactance and a resistance. Based on such measurements, we estimate that for our system, $\alpha = R_c/\omega M \sim 0.1$, a plausible value.

2. Heat leaks between engines

We now briefly discuss another complication: heat flowing between neighboring prime movers due to a temperature difference that develops as a result of mass coupling. Imagine that in a given locked state, engine I becomes ''loaded,'' feeding power into engine II, which is then ''driven.'' The amplitude P_{I} in engine I will fall and its hot temperature $T_{\mathrm{H,I}}$ will rise; conversely, P_{II} will rise and $T_{\mathrm{H,II}}$ will fall. If the two hot ends have some thermal contact, a heat leak $\dot{Q}_{\mathrm{cross}} = UA(T_{\mathrm{H,I}} - T_{\mathrm{H,II}})$ will flow between them, where UA is some effective heat-transfer coefficient. This has the effect of draining more power from engine I and feeding more into engine II, making the amplitude imbalance between the engines that much greater. Hence, it makes $\partial P^2/\partial \dot{W}_L$ greater than it would otherwise be, making Q larger and enhancing the coupling. This additional coupling will not be apparent when making a load measurement on a single engine, unless great care is taken to duplicate the conditions of the coupled state (e.g., pump the gas out of the other engine so it cannot start, and manipulate its heat input so it always has the T_{H} that it would have in the locked state corresponding to the first engine's P).

This also points to a larger issue: the effect of different modes of operation on engine coupling. Engines may be run with constant power, constant hot-end temperature, or something in between (such as constant pressure amplitude, or constant power delivered to a load, etc.) The general principles developed so far should still apply; that is, if one can find the ''Q'' that characterizes the engines in their typical mode of operation, along with the effective moving gas mass and the case mass, one should be able to estimate the coupling strength. Care must be taken, of course, to always reexamine the energy balance whenever the mode of operation is changed. For instance, consider two mass-locked engines whose hot-end and cold-end stack temperatures are held constant. This example is of interest because material properties usually limit how hot an engine may be run, and the need for maximum power density and efficiency may require that the engine be run at this upper limit. If one such engine experiences an extra load as a result of being mass-coupled to another engine, its hot temperature will tend to rise and its oscillating pressure amplitude will fall; the temperature control will decrease the power flowing to that engine to maintain its temperature at the upper limit, lowering the pressure still further. Thus one might expect that such engines would have very high $\partial P^2/\partial \dot{W}_L$, and hence high Q, implying that they would allow very little phase shift for a given difference in natural frequency [see Eq. (19)]; this behavior is indeed observed in simulations. However, the engines allow large differences in pressure amplitude for small frequency differences.

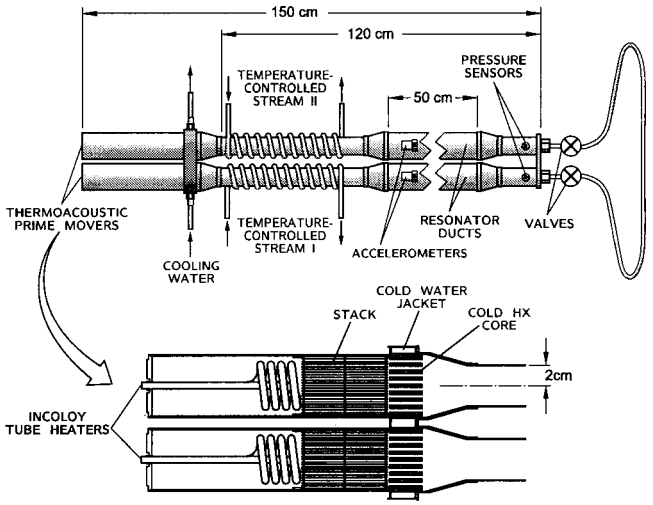

FIG. 4. Experimental setup for exploring the behavior of coupled thermoacoustic engines. The insulation surrounding the prime movers and the temperature-control coils is not pictured.

Having given the reader a taste of the challenges involved in making a good mass-locking measurement, we will proceed to describe our experiments with small, mass-coupled thermoacoustic engines.

IV. APPARATUS AND EXPERIMENTS

To explore mass-locking of acoustic engines experimentally, we use two nearly identical thermoacoustic engines which are rigidly attached side by side (these are the same engines that were used for a portion of the acoustic coupling work described in Ref. 3). Two neighboring ends of the engines are connected by a coupling duct which can be inserted or removed from the system by means of valves, enabling the system to be acoustically coupled, or not, as desired. Each engine consists of a section of duct of varying cross section (the resonator) connected to a thermoacoustic prime mover, by which we mean an electric heater, a water-cooled heat exchanger, and a stack of parallel plates between them; these sustain the oscillations in the resonator when the engine is running.

Figure 4 shows the essentials of the experimental setup, and some details of the thermoacoustic prime mover hardware. Note that the engines share a water jacket that cools their cold heat exchangers, and both are welded to a common plate at the other end. The engines are also joined by two narrow, 50-cm-long plates that are welded between the 50-cm-long ''fat'' sections of the resonators. A section of each resonator is wrapped with copper refrigeration tubing, which circulates water from a temperature-controlled bath. Thus the gas temperature in each engine can be varied independently, enabling control of $\Delta\omega$. A pressure sensor is mounted at the end of each resonator where it joins the coupling duct. We

take the signal from the sensor in resonator I (pressure sensor I) to represent $p_1(t)$, and that from pressure sensor II to represent $p_{II}(t)$. Using p_1 as a reference to a lock-in amplifier and using p_{II} as the input signal allows a direct measurement of ϕ. Independent monitoring of pressure sensors I and II gives $P_1(t)$ and $P_{II}(t)$. Accelerometers on the cases measure case vibration in the axial (x) direction, and numerous thermocouples (not pictured) provide temperature data on the gas near the hot end of the stack, the cooling water, the water in the coils wound around the resonators, and the gas inside the resonators. Multimeters monitor the input voltages and currents to the tube heaters that power the engines. The accelerometers are used to verify that the two engines, welded together, act like a rigid structure, and that vibrations are indeed canceled when the phase between the engines approaches π—we find that cancellation of case vibration is at least 99.5% complete when $\phi=\pi\pm0.002$. The engines are filled with xenon, with the mean pressure $p_m=303$ kPa; they run at 50 Hz, in a room temperature environment (rejecting heat at 300 K). The combined case mass of the engines, including water in the heat exchangers and such, is $M\simeq11$ kg.

To assist us in interpreting our data, we simulate the system using DELTAE. We use a single simulated engine, without moving endcaps, to help us estimate μ and Q for the system; we use a pair of simulated engines, whose combined case mass moves in response to the oscillating pressure, to compare simulated mode-locked states with measured ones. The simulated mode-locked system involves a few approximations; for instance, the forces on the heat exchangers and stacks are neglected, and the changes in cross-section are all treated as abrupt (including the truncated cones shown in Fig. 4). Nevertheless, we expect that the agreement between experiment and simulation should be reasonable.

The single simulated engine is used to estimate $w(x)$, the pressure waveform in the engines. The only pressure reading taken in each experimental engine is at the end of the resonator (the ''cold end''), as shown in Fig. 4, so we trust DELTAE's linear acoustics to estimate what the pressure distribution in a given geometry should be. Combined with our knowledge of $A(x)$, this allows us to numerically carry out the integrals in Eqs. (32) and (35).

To obtain Q, we also need $\partial P^2/\partial\dot{W}_L$. To measure this quantity experimentally, we use a precision leak valve in series with a small cylindrical ''tank'' of volume $V=150$ cm^3 to form an acoustic RC load, and attach this load to the end of one engine resonator at a time, observing changes in the end pressure of that engine as the valve is gradually opened. The other engine is pumped out for this measurement, so it cannot start; some heat is still applied to it, however, to maintain it near the temperature it would have *if* it were running. The actual power dissipated at each valve setting is estimated by using a pressure transducer within the tank, along with the one at the end of the engine, to measure the pressure difference across the valve. This pressure difference and the tank volume V are used to calculate the dissipated power according to[13] $\dot{W}_L=\omega V|p||p_T|\sin\theta/2\gamma p_m$, where p is the oscillating pressure at the end of the engine, p_T is the pressure in the tank, and θ is the phase by which p leads p_T.

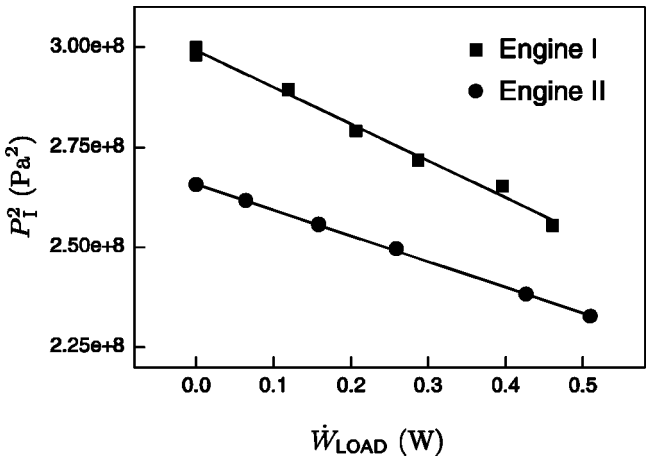

FIG. 5. Load responses of the engines used in the mass-locking experiment. The squares are engine I data and the circles, engine II; the lines are linear fits. Each data set on a given engine was taken with the neighboring engine hot, but not running, to approximate the heat leak that exists when both engines are running.

In these measurements, we not only had to contend with heat leaks between the engines, as discussed earlier, but also ordinary heat leaks from the engines to the ambient. Rather than attempt to subtract the ambient heat leaks from the electric power going into the engines and manipulate the electric power to maintain constant heat input, we chose to simply maintain constant electric power, and characterize the load performance of the engines as they were, leaks and all. Figure 5 shows the results; evidently $\partial P^2/\partial\dot{W}_L$ is fairly linear in the region studied, but the data have sufficient scatter that a higher-order fit is probably not warranted. The data for each engine were taken over the range of pressures which that engine experienced when the data on locked states were taken. Of interest is the difference in slopes between I and II; apparently the two engines do not perform identically, despite being constructed ''identically.'' One difficulty in predicting the performance of these particular engines, and in modeling them, is the use of tubular heaters in the prime movers (see detail in Fig. 4). These heaters are robust and easy to bend into a desired shape, but are not as well understood thermodynamically as standard shell-and-tube or parallel-plate heat exchangers.

We find that $Q_1=73$ and $Q_{II}=50$, with $\overline{Q}$, the average, being 62; by simulating this measurement in DELTAE, we find $Q=61$. Because of the difficulties in precisely modeling the hot ends of these engines, and the large difference between Q_1 and Q_{II}, this striking agreement must be a bit coincidental. The difference in measured Q between the engines adds a slight offset of order $[(Q_{II}-Q_1)/\overline{Q}]^2$ to Eq. (17). We do not treat the question of the offset rigorously, but merely measure it and subtract it from our simulated and theoretical results.

We may also use an experimental observation to obtain an approximate value for μ, the effective mass ratio. Observing the engines when they are coupled but not mode-locked, and measuring the frequency and phase of both engines as a

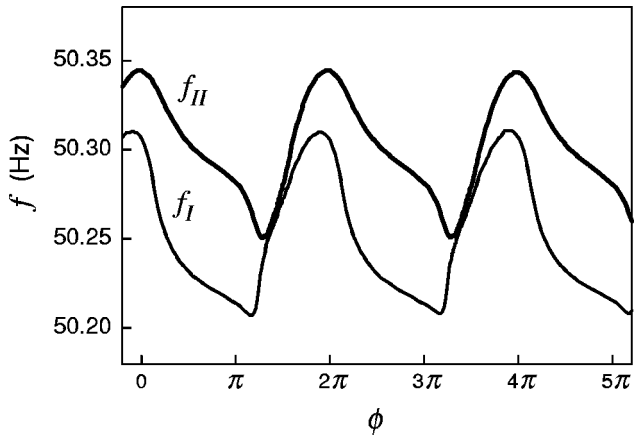

FIG. 6. Frequency as a function of the phase between two mass-coupled engines that are on the verge of locking.

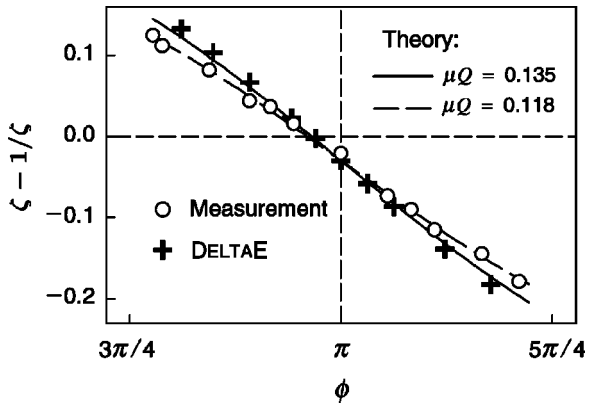

FIG. 7. Amplitude imbalance $\zeta - 1/\zeta$, where $\zeta = P_{\mathrm{II}}/P_{\mathrm{I}}$, versus phase difference ϕ of mass-locked state. Circles are data points, crosses are DELTAE simulations, and the broken line is a fit to $\zeta - 1/\zeta = 2\mu Q \sin\phi + C$, with μQ and C free parameters. The solid line is the same equation, but using our estimated μ and Q. The difference in their slopes at $\phi = \pi$ is about 15%. The DELTAE points have had the offset C subtracted from them as well.

function of time, one may obtain a plot of frequency versus phase for the engines as they beat. Such a plot is shown in Fig. 6; note that the frequencies are their lowest near $\phi = \pi, 3\pi, 5\pi, \ldots$ and their highest near $\phi = 0, 2\pi, 4\pi, \ldots$, consistent with the idea that a moving case shifts frequencies up. By comparing the high and low values, we find that the frequency shift $|\Delta f|/f \approx 0.002$; if we assume $f^2 = f_0^2(1+\mu)$, then $\mu \approx 0.004$. Since this includes the moving gas in two engines, we may guess that μ for one engine, that is, the $\mu = m/M$ to use in Eqs. (17) and (18), is μ (expt.) ≈ 0.002. Using our theory, together with our DELTAE model to find $w(x)$, we find that the effective mass $m = 0.024$ kg for our engines; with $M = 11$ kg, μ (theo.) ≈ 0.0022.

We are now poised to predict $\zeta - 1/\zeta$ versus ϕ for our engines; we choose $\mu Q = 0.0022 \times 62 = 0.135$ as our ''theoretical'' coefficient in Eq. (17). This equation can be compared to actual phase differences and amplitude ratios at various locked states for our engines. We found that the engines would readily mode-lock, and the phase could be varied easily by changing the temperature of one of the cooling coils; however, we found that the states were not particularly stable, but very sensitive to small changes in temperature. Only by very carefully ''teasing'' the system could it be made to settle at a particular state (largely because the hot temperatures need to equilibrate to establish a stable state). Figure 7 shows a comparison between theory and experiment. Considering all the approximations that have been made to get to this point, the agreement between the three methods is remarkably good.

We also try to compare theory and experiment for Eq. (19), but here we must grapple with the difficulty in measuring $\Delta\omega$. The most straightforward way to measure the difference in frequency between two coupled engines is to decouple them and measure the beat frequency; however, we know from Sec. III that this frequency difference is not necessarily the ''natural frequency difference'' required by theory. In addition, when the engines are decoupled, the hot-end temperatures immediately begin to shift, making the measurement of a long beat period somewhat difficult. We have chosen an indirect, but simpler, method to find $\Delta\omega \approx \Omega_{\mathrm{II}} - \Omega_{\mathrm{I}}$. We record phase versus $\Omega_{\mathrm{II}} - \Omega_{\mathrm{I}}$ for the engines when they are *acoustically* coupled, using the coupler that is already in place. An extra 130 kg of mass is clamped to the engines during the acoustic measurement, to remove all effects of mass-coupling. Subsequently, during the mass-locking measurement, after the engines have established a stable mass-locked state we momentarily open the acoustic coupler valves and record the phase, which can then be related to a frequency difference. Figure 8 shows a plot of ϕ_A, the phase at which the system is mode-locked due to acoustic coupling, versus the normalized frequency difference $\Delta\omega/\omega \approx (\Omega_{\mathrm{II}} - \Omega_{\mathrm{I}})/\omega$. Near $\phi_A = \pi$, the data are linear, and we use the slope in this region to obtain the relationship between ϕ and $\Omega_{\mathrm{II}} - \Omega_{\mathrm{I}}$. We have chosen a relatively narrow-diameter coupler for this part of the work, so that the acoustic coupling is fairly weak (although not as weak as the mass coupling). Thus the phase of the acoustically locked state is a sensitive measure of frequency difference. We allow the engines to lock through mass coupling (i.e., with the acoustic coupler's valves closed), record the steady-state amplitudes and phases, and then throw the valves open momentarily and record the phase ϕ_A, thus obtaining $\Omega_{\mathrm{II}} - \Omega_{\mathrm{I}}$. As

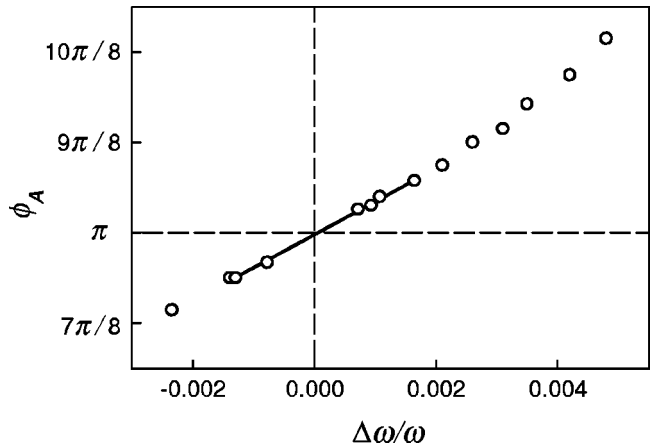

FIG. 8. The phase of the locked state when the engines are acoustically coupled, achieved when the coupler valves in Fig. 4 are open, versus the frequency difference estimated by measuring the beat period when the valves are closed. In this measurement, an extra 130 kg of mass is clamped to the engines, to discourage any mass-coupling.

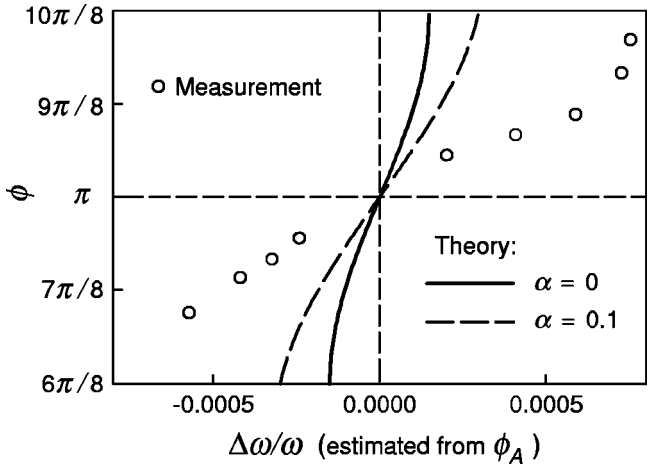

FIG. 9. The phase difference of the mass-locked state versus the frequency difference estimated from the corresponding acoustically-locked state. The quantity α is defined in Sec. III A 1, and represents the degree of external dissipation in the system, such as that caused by friction in the supports.

expected, we find that ϕ_A drifts, since the hot temperatures drift as soon as the valves are closed, and thus $\Omega_{\mathrm{II}}-\Omega_{\mathrm{I}}$ is a moving target. We find that measuring the phase about 5 s after the valves are opened gives a repeatable, if not wholly accurate, value for ϕ_A.

Figure 9 shows our mass-locked ϕ vs $\Delta\omega/\omega$ data, compared with two theoretical predictions—one assuming no external dissipation, and another assuming moderate external dissipation. We were able to achieve mass-locking only between $3\pi/4<\phi<5\pi/4$; this is in contrast to the acoustically coupled engines studied in Ref. 3, which would lock between $\pi/2<\phi<3\pi/2$. We may use our theory to predict the capture bandwidth; starting with Eq. (18), we ask what angle ϕ makes $\Delta\omega$ a maximum. This is equivalent to seeking ϕ such that $d(\sin\phi\cos\phi)/d\phi=0$. This occurs when $\phi=(2n+1)\pi/4$, $n=0,1,2,\ldots$, and hence when $\sin\phi\cos\phi=\frac{1}{2}$. For a system whose band center is nominally at $\phi=\pi$, then, we predict

$$\pm\left(\frac{\Delta\omega}{\omega}\right)_{\max}=\pm\frac{\mu^2 Q}{2}\quad\text{at}\quad\phi=\pi\pm\frac{\pi}{4}. \tag{45}$$

The experimental phase limits agree well with this prediction, but the predicted frequency bandwidth is much narrower.

The shapes of the experimental and theoretical curves have some qualitative similarities, but as expected (recall Fig. 2), the slope of the experimental curve is much less than that predicted by theory. We found that measuring ϕ_A ''immediately'' (within 0.5 s) after the valves were opened appeared to approximately double the slope; however, the valves were operated by hand and took several tenths of a second to open, so these data are of dubious value. While the simplest theory (no dissipation) predicted that the mass-coupling in our system should have been about 25 times weaker than the acoustic coupling, the data suggest it is only about 10 times weaker. External dissipation brings these numbers into closer agreement, as shown by the dashed line in Fig. 9, but it would require three times as much dissipation as we estimate for our system to make the experimental and theoretical curves coincide. We believe inability to measure the ''true'' value of $\Delta\omega/\omega$ is the biggest source of error.

Since $\Delta\omega/\omega$ is of mostly theoretical interest anyway, we consider what effect objective changes might have on our system. The DELTAE model, which agrees well with theory and experiment as demonstrated by Fig. 7, suggests that a 0.03-K change in the resonator gas temperature of one engine, within the section wrapped in copper tubing, would cause a change in phase angle $\Delta\phi=\pi/16$. The measurement of gas temperature in our experiment was too coarse to verify this, but if we assume it is correct, it demonstrates again how very sensitive mass-coupled engines are, compared to the acoustic coupling necessary to cancel vibration. For comparison, consider an acoustically coupled system of two engines, designed so that 95% of the case vibration is canceled when $\Delta\omega/\omega=0.01$. This implies $|\Delta\phi|=|\phi-\pi|\leqslant 0.05$ when the difference in resonator gas temperatures is $\Delta T/T_m=0.02$, or $\Delta T=6$ K if the mean temperature T_m is about 300 K. For such a system, $(T_m/\pi)\Delta\phi/\Delta T\approx 1$; for our mass-locked system, $(T_m/\pi)\Delta\phi/\Delta T\approx 600$.

In conclusion, we have shown that the Huygens effect, or mass-coupling, is sufficiently weak in thermoacoustic engines that it may be ignored in many circumstances, although a precise measure of its weakness will often be difficult to obtain. It is also apparent that the natural mode for the engines to mass-lock has the correct phase relationship to minimize motion of the common mass. This is further encouragement that mass-locking will not interfere with the canceling of engine vibrations by acoustic coupling.

There are some circumstances, of course, where the mass-coupling could be significant. Engines that use a liquid as the working fluid (such as a liquid-sodium thermoacoustic engine[6]) could have $\mu\sim 1$. This could also be true of acoustic engines whose resonators include moving parts, such as magnets for generating electricity. This strong coupling might in fact be an advantage, if the proper suspension or supports for the engines can encourage them to lock in antiphase, thus lessening or eliminating the need for any acoustic coupling.

ACKNOWLEDGMENTS

The authors wish to thank Bob Keolian and Bob Ecke for teaching us about mode-locking; Bill Ward, Scott Backhaus, and Bob Hiller for useful discussions; and David Gardner for assistance with the experiments. We are also grateful to Andrew Piacsek (of Central Washington University) for providing an English translation of Huygens' letter. This work has been supported by the Office of Basic Energy Sciences in the U.S. Department of Energy.

[1] C. Huygens, in *Ouevres Completes de Christian Huyghens*, edited by M. Nijhoff (Societe Hollandaise des Sciences, The Hague, The Netherlands, 1893), Vol. 5, p. 243 (a letter to his father, dated 26 Feb. 1665).
[2] G. W. Swift, ''Thermoacoustic natural gas liquefier,'' in Proceedings of the DOE Natural Gas Conference, Houston, TX, March 1997.
[3] P. S. Spoor and G. W. Swift, ''Mode locking of acoustic resonators and its application to vibration cancellation in acoustic heat engines,'' J. Acoust. Soc. Am. **106**, 1353–1362 (1999).

[4] A. B. Pippard, *The Physics of Vibration (Omnibus Edition)* (Cambridge U. P., Cambridge, 1989), p. 392.
[5] B. Van der Pol, ''The nonlinear theory of electric oscillations,'' Proc. Inst. Radio Engineers **22**, 1051 (1934).
[6] G. W. Swift, ''Thermoacoustic engines,'' J. Acoust. Soc. Am. **84**, 1145–1180 (1988).
[7] A. B. Pippard, *The Physics of Vibration (Omnibus Edition)* (Cambridge U.P., Cambridge, 1989), Chap. 12.
[8] P. M. Morse, *Vibration and Sound* (American Institute of Physics, New York, 1986), pp. 104, 313.
[9] J. W. Strutt and Lord Rayleigh, *Theory of Sound* (Dover, New York, 1945), Vol. 1, Sec. 88.
[10] A. D. Pierce, *Acoustics: An Introduction to Its Physical Principles and Applications* (Acoustical Society of America, Woodbury, New York, 1989), p. 53.
[11] W. C. Ward and G. W. Swift, ''Design environment for low amplitude thermoacoustic engines (DeltaE),'' J. Acoust. Soc. Am. **95**, 3671–3672 (1994). Fully tested software and user's guide available from Energy Science and Technology Software Center, US Department of Energy, Oak Ridge, TN. To review DeltaE's capabilities, visit the Los Alamos thermoacoustics web site at `http://www.lanl.gov/thermoacoustics`. For a beta-test version, contact ww@lanl.gov (Bill Ward) via Internet.
[12] N. Rott, ''Thermoacoustics,'' Adv. Appl. Mech. **20**, 135–175 (1980).
[13] A. M. Fusco, W. C. Ward, and G. W. Swift, ''Two-sensor power measurements in lossy ducts,'' J. Acoust. Soc. Am. **91**, 2229–2235 (1992).